Supplementary Information

The Network Architecture of Cortical Processing in Visuo-spatial Reasoning

Ehsan Shokri-Kojori,[a*] Michael A. Motes,[a,b] Bart Rypma,[a,b] Daniel C. Krawczyk,[a,b]

[a]Center for BrainHealth, School of Behavioral and Brain Sciences, The University of Texas at Dallas, Dallas, TX, 75235-7205, USA
[b]Department of Psychiatry, University of Texas Southwestern Medical Center, Dallas, TX, 75390-9070, USA

[*]To whom correspondence may be addressed: Ehsan Shokri-Kojori
Center for BrainHealth, School of Behavioral and Brain Sciences, The University of Texas at Dallas, Dallas, TX, 75235-7205, USA
E-mail: *shokri@utdallas.edu*, Phone: 214-905-3007, Fax: 214-905-3026

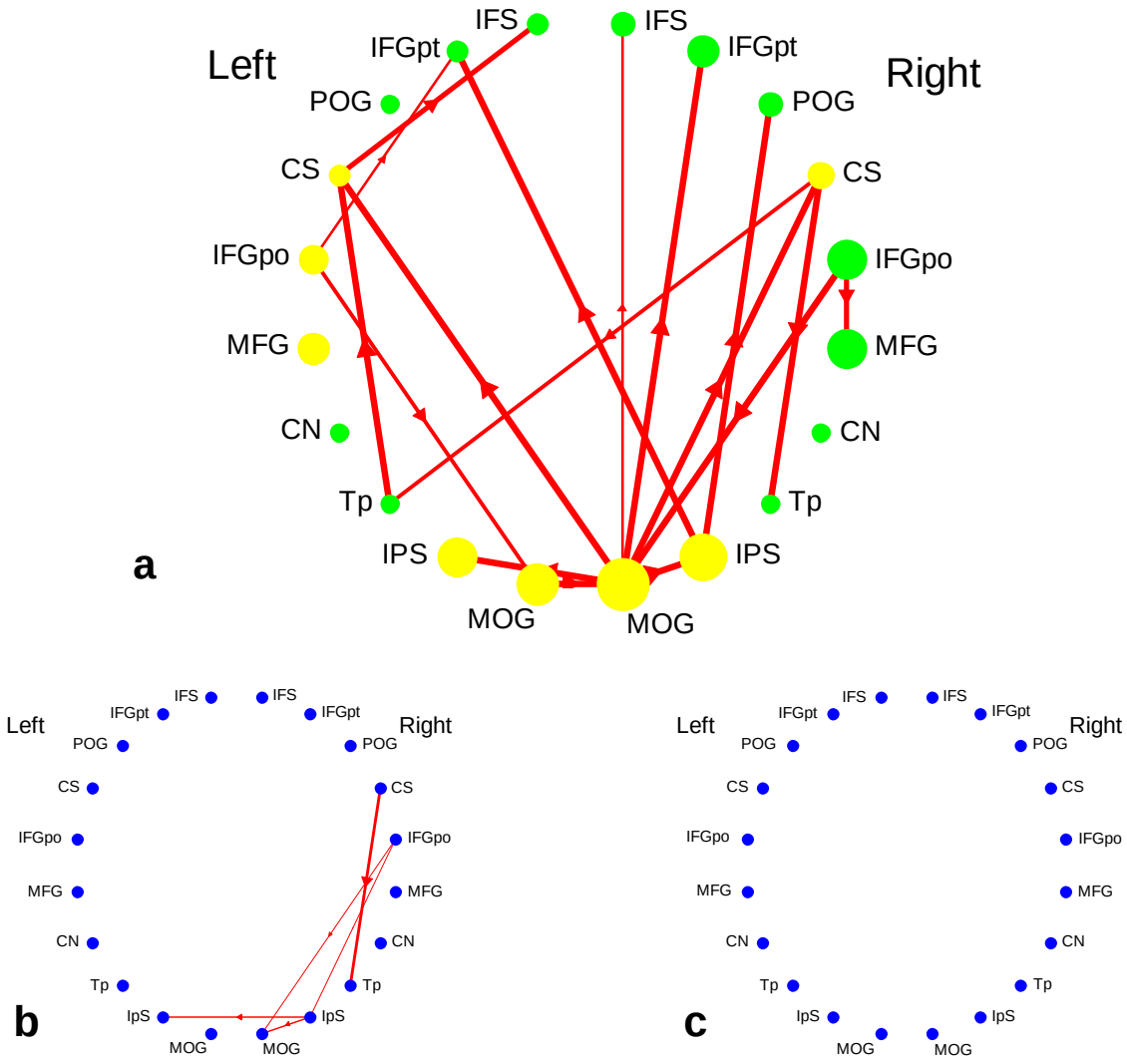

Supplementary Figure S1. Connectivity contrast for ROI pairs. (a) Each arrow shows the dominant direction of influence in ROI pairs with significant group-level connectivity. A paired sample *t*-test on the causal correlations was performed to contrast the connectivity measures at the group-level ($P < 0.05$). Yellow circles represent demand-sensitive ROIs with significant correlations between activity and RT changes (FDR, $P < 0.05$). Green circles represent non-significant correlations with RT. The radius of the circles is proportional to the mean *t*-value of selected voxels within each ROI across all task conditions. (b) Group-level connections that are more reliable when fast performers are compared to slow performers through a one-tailed *t*-test on the causal correlations for each ROI pair ($P < 0.05$). (c) No connection was found to be significantly more reliable when slow performers were compared to fast performers.

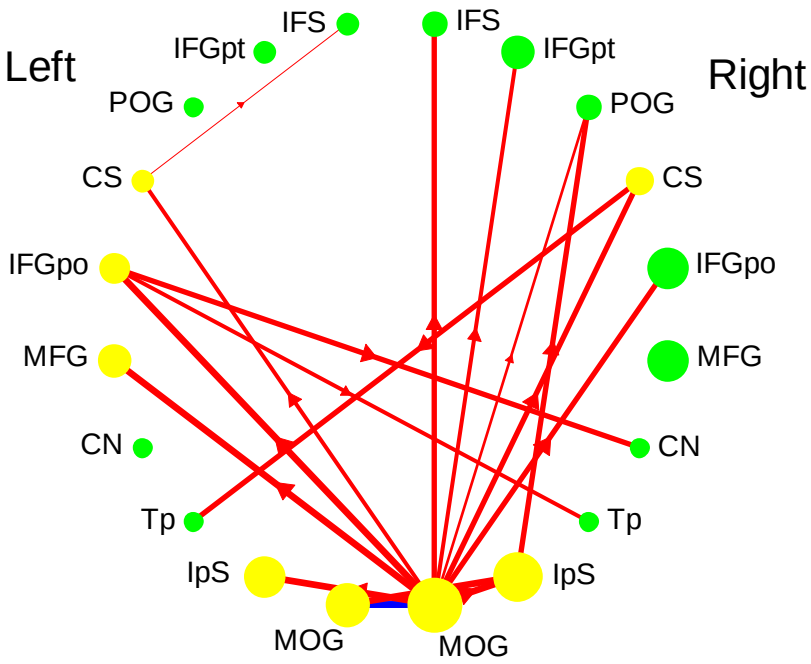

Supplementary Figure S2. Interhemispheric contrast map of the connectivity patters. Each arrow shows a significant connection when contrasted by the homologous connection in the contralateral hemisphere. A paired sample *t*-test on the causal correlations was performed to contrast the connectivity measures at the group-level ($P < 0.05$). Yellow circles represent demand-sensitive ROIs with significant correlations between activity and RT changes (FDR, $P < 0.05$). Green circles represent non-significant correlations with RT. The radius of the circles is proportional to the mean *t*-value of selected voxels within each ROI across all task conditions.

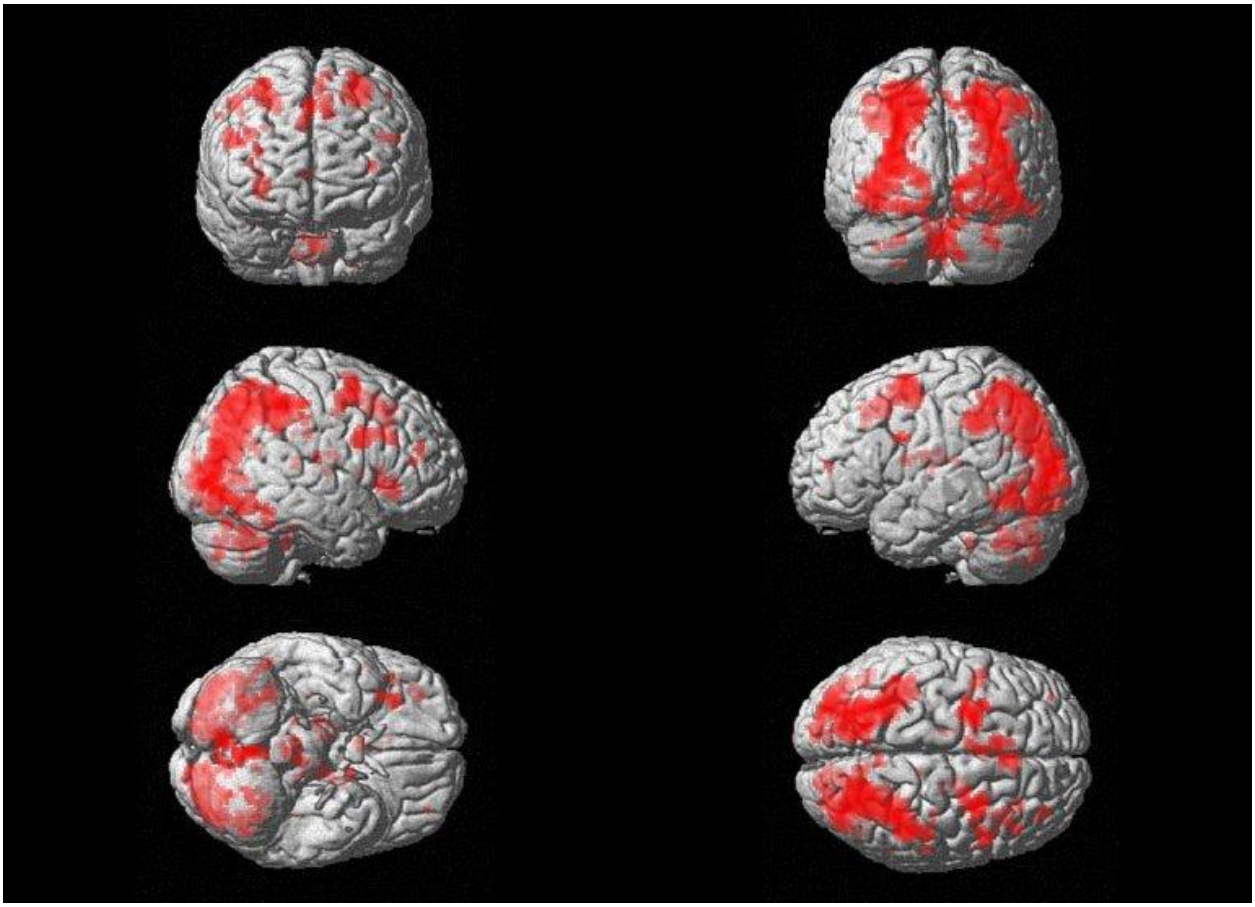

Supplementary Figure S3. Contrast map between 3 and 1 relational complexity levels (FDR, $P < 0.05$, cluster threshold = 5).

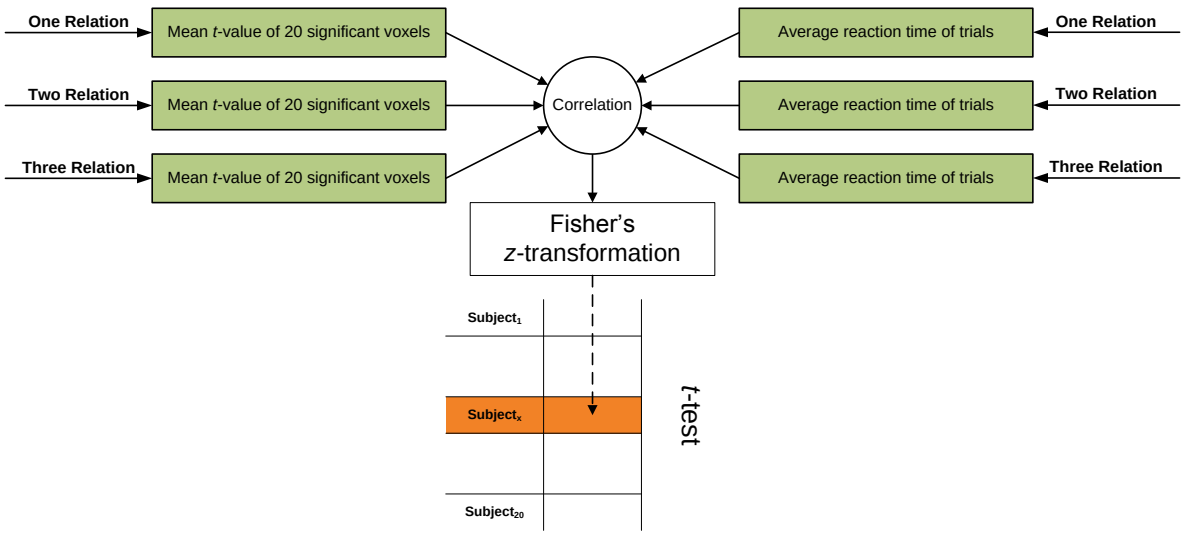

Supplementary Figure S4. Schematic of the analysis performed at the subject-level to examine whether the ROI activity (measured by RT) at each task condition is correlated with the corresponding average RT. Multiple comparison correction was performed using False Discovery Rate (FDR) method[S5].

Coordinates	Mean (mm)	Standard Deviation (mm)	MGF ROIs from this study (mm)
Left Hemisphere			
X	-32	11	-40
Y	-4	4	0
Z	50	4	50
Right Hemisphere			
X	31	11	30
Y	-4	5	0
Z	51	5	54

Supplementary Table S1. Average coordinates of FEF across multiple studies[S4] converted to the MNI space compared to FEF coordinates estimated in this study (http://imaging.mrc-cbu.cam.ac.uk/imaging/MniTalairach).

ROI Name	Description	X Y Z	Brodmann Area
LCN	Left Caudate Nucleus	-16 -7 16	-
LCS	Left Cingulate Sulcus	-11 20 40	32,8
LIFGpo	Left Inferior Frontal Gyrus (pars opercularis)	-42 6 26	44
LIFGpt	Left Inferior Frontal Gyrus (pars triangularis)	-46 28 34	45
LIFS	Left Inferior Frontal Sulcus	-26 50 8	10
LIpS	Left Interaparietal Sulcus	-34 -46 38	40
LMFG	Left Middle Frontal Gyrus	-40 0 50	6
LMOG	Left Middle Occipital Gyrus	-26 -70 28	7,19
LPOG	Left Posterior Orbital Gyrus	-26 28 -12	47
LTp	Left Thalamus (pulvinar)	-14 -28 12	-
RCN	Right Caudate Nucleus	18 -4 16	-
RCS	Right Cingulate Sulcus	10 20 44	32,8
RIFGpo	Right Inferior Frontal Gyrus (pars opercularis)	50 10 26	44
RIFGpt	Right Inferior Frontal Gyrus (pars triangularis)	46 32 26	45
RIFS	Right Inferior Frontal Sulcus	26 44 12	10
RIpS	Right Interaparietal Sulcus	34 -44 40	40
RMFG	Right Middle Frontal Gyrus	30 0 54	6
RMOG	Right Middle Occipital Gyrus	32 -74 24	39,19
RPOG	Right Posterior Orbital Gyrus	34 28 -4	47
RTp	Right Thalamus (pulvinar)	20 -30 10	-

Supplementary Table S2. Functional ROIs generated by contrasting 3 and 1 relational complexity levels (FDR, $P < 0.05$, cluster threshold = 5).

Supplementary Methods

Performance correlations between the visuo-spatial reasoning task and RPM problems

We tested an additional thirty-two participants outside the scanner. These subjects performed both VSRT and a set of 12 advanced RPM problems. If VSRT is representative of contributing reasoning processes involved in RPM, we expected consistent accuracy and/or RT correlations between the RPM and our level 1, 2, and 3 problems. We obtained a range of RPM scores (Accuracy: *M* = 58.90%, *SD* = 20.84%; RT: *M* = 45.64s, *SD* = 19.24s). Results of the VSRT were similar to those of the fMRI subjects in accuracy (1-relation *M* = 94.53%, *SD* = 17.34%; 2-relation *M* = 92.97%, *SD* = 18.90%; 3-relation *M* = 90.82%, *SD* = 17.79%) and RT (1-relation *M* = 4085.49ms, *SD* = 1279.46ms; 2-relation *M* = 4164.85ms, *SD* = 1272.37ms; 3-relation *M* = 4848.87ms, *SD* = 1779.22ms). We found significant correlations between accuracy on the RPM and each level of complexity: RPM and 1-relation (*r* = 0.31, *P* = 0.037); RPM and 2-relation (*r* = 0.34, *P* = 0.025); RPM and 3-relation (*r* = 0.36, *P* = 0.018). Notably, the two tasks are not extremely well-correlated, as we would predict based on the assumption that the RPM is comprised of multiple subcomponents with relational integration being one of them. Larger correlations were observed between response times on the RPM and VSRT: RPM and 1-relation (*r* = 0.50, *P* = 0.001); RPM and 2-relation (*r* = 0.57, *P* = 0.0002); RPM and 3-relation (*r* = 0.52, *P* = 0.0008). The results demonstrated the relationship between performance on each VSRT condition and the RPM. The consistency in the strength of correlations between performance measures on our task and RPM indicates a considerable overlap between the contributing cognitive resources.

Implementation of the Granger causality technique

Let $\mathbf{x}$, $\mathbf{y}$ be two vector stationary time-series with zero means. The prediction of $\mathbf{y}$ from past of $\mathbf{x}$ considering $\boldsymbol{U}$ as the time-series matrix of other possible interacting ROIs, could be formulated as the following (the full model):

$$\mathbf{y}_t = \sum_{l=1}^{L} \boldsymbol{A}_l \boldsymbol{U}_{t-l} + \sum_{l=1}^{L} \mathbf{b}_l \mathbf{y}_{t-l} + \sum_{l=1}^{L} \mathbf{c}_l \mathbf{x}_{t-l} + \boldsymbol{\varepsilon}_t^{Uyx},$$

where $\boldsymbol{\varepsilon}_t^{U,y,x}$ is the error term when past information from $\boldsymbol{U}$, $\mathbf{x}$ and $\mathbf{y}$ are used in the prediction model. $\boldsymbol{A}_l$, $\mathbf{b}_l$ and $\mathbf{c}_l$ are selected to minimize the variance of the prediction error. The lag length, L, determines the farthest past time point to be included in the model. If $\mathbf{x}$ has a unique causal influence on $\mathbf{y}$ then excluding $\mathbf{x}$ from the full model should increase the variance of prediction error. In the reduced model we have:

$$\mathbf{y}_t = \sum_{l=1}^{L} \boldsymbol{D}_l \boldsymbol{U}_{t-l} + \sum_{l=1}^{L} \mathbf{e}_l \mathbf{y}_{t-l} + \boldsymbol{\varepsilon}_t^{U,y},$$

where $\boldsymbol{\varepsilon}_t^{U,y}$ is the prediction error when only past time-series from $\boldsymbol{U}$ and $\mathbf{y}$ are included in the prediction model. $\boldsymbol{D}_l$ and $\mathbf{e}_l$ are selected to minimize the variance of the prediction error. The relative reduction in variance of prediction error between full and reduced models is used to formulize the causal relationship as a measure of linear feedback[S1].

$$F_{x \to y} = \log \frac{\mathrm{var}(\boldsymbol{\varepsilon}_t^{U,y})}{\mathrm{var}(\boldsymbol{\varepsilon}_t^{U,y,x})},$$

The lag length (model order) is determined based on a tradeoff between model complexity and the reduction in error variance using the Bayesian Information Criterion method[S2]. Given that the underlying neuronal interactions that give rise to the hemodynamic responses are fast and happen within fractions of TR, the precedence of time-series should not be reflected in time points farther than one sample away. Moreover, prior studies have shown that the model order of 1 was optimal in both simulations and exploratory analyses for fMRI data[S1]. Limiting the model order to $L = 1$ motivates formulizing the causal influence of $\mathbf{x}$ on $\mathbf{y}$, $I_{\mathbf{x} \to \mathbf{y}}$, as the correlation between the error term of reduced model and the past of $\mathbf{x}$ time-series. The causal influence is related to the proportion of variance of the error term in the reduced model that could be uniquely explained by past $\mathbf{x}$ time-series:

$$I_{x \to y} = \frac{SC(\boldsymbol{\varepsilon}_t^{U,y}, \mathbf{x}_{t-1})}{\sqrt{SS(\boldsymbol{\varepsilon}_t^{U,y}) \times SS(\mathbf{x}_{t-1})}},$$

where *SC* represents sum of cross products and *SS* represents sum of squares. Given that the casual influence is calculated through a correlation analysis, applying Fisher's *z*-transformation will adjust the distribution of those correlation coefficients to be suitable for averaging the results across runs and performing group-level *t*-tests[S3] (see Fig. 3 for more details).

Supplementary References

S1. Roebroeck, A., Formisano, E. & Goebel, R. Mapping directed influence over the brain using Granger causality and fMRI. *Neuroimage* **25**, 230–242 (2005).
S2. Schwartz, G. Estimating the dimension of a model. *Ann. Stat.* **5**, 461–464 (1978).
S3. Fisher, R. Frequency distribution of the values of the correlation coefficient in samples of an indefinitely large population. *Biometrika* **10**, 507–521 (1915).
S4. Paus, T. Location and function of the human frontal eye-field: A selective review. *Neuropsychologia* **4**, 475–483 (1996).
S5. Benjamini, Y. & Yekutieli, D. The control of the false discovery rate in multiple testing under dependency. *Ann. Statist.* **29**, 1165–1188 (2001).